energies

MDPI

Article

Optimization Design of the Impeller Based on Orthogonal Test in an Ultra-Low Specific Speed Magnetic Drive Pump

Fei Zhao [1,2], Fanyu Kong [1,*], Yisong Zhou [1], Bin Xia [2] and Yuxing Bai [3]

1 National Research Center of Pumps, Jiangsu University, Zhenjiang 212013, China; zhaof@wxit.edu.cn (F.Z.); m13215555321@163.com (Y.Z.)
2 School of Mechanical Technology, Wuxi Institute of Technology, Wuxi 214121, China; xia_bin2007@126.com
3 School of Automotive & Rail Transit, Nanjing Institute of Technology, Nanjing 211167, China; yxbai1012@163.com
* Correspondence: kongfy2918@sohu.com

Received: 19 October 2019; Accepted: 10 December 2019; Published: 13 December 2019

Abstract: To improve the hydraulic performance in an ultra-low specific speed magnetic drive pump, optimized design of impeller based on orthogonal test was carried out. Blades number Z, bias angle in peripheral direction of splitter blades θ_s, inlet diameter of splitter blades D_{si}, and deflection angle of splitter blades α were selected as the main factors in orthogonal test. The credibility of the numerical simulation was verified by prototype experiments. Two optimized impellers were designed through the analysis of orthogonal test data. The internal flow field, pressure fluctuation, and radial force were analyzed and compared between optimized impellers and original impeller. The results reveal that impeller 7 (Z = 5, θ_s = 0.4θ, D_{si} = 0.75D_2, α = 0°) could increase the head and efficiency, compared to the original impeller, by 2.68% and 4.82%, respectively. Impeller 10 (Z = 5, θ_s = 0.4θ, D_{si} = 0.55D_2, α = 0°) reduced the head by 0.33% and increased the efficiency by 8.24%. At design flow rate condition, the internal flow of impeller 10 was the most stable. Peak-to-peak values of pressure fluctuation at the volute tongues of impeller 7 and impeller 10 were smaller than those of the original impeller at different flow rate conditions (0.6 Q_d, 1.0 Q_d and 1.5 Q_d). Radial force distribution of impeller 10 was the most uniform, and the radial force variance of impeller 10 was the smallest.

Keywords: ultra-low specific speed magnetic drive pump; orthogonal test; splitter blades; optimized design; pressure fluctuation; radial force

1. Introduction

With the characteristics of no leakage and compact structure, magnetic drive pumps are widely used in aerospace, chemical, pharmaceutical, and military industries [1–4]. The efficiency of magnetic drive pumps is usually lower than that of ordinary mechanical seal pumps. Therefore, improving its efficiency is of great significance for saving energy and reducing environmental pollution.

In recent years, research has been conducted on the influence of splitter blades on performance and internal flow of pumps. ХлопеНКоВ.п.р[5] improved head and efficiency by welding short blade structures on the impeller. The research results of Kergourlay G et al. [6] found that the internal velocity and pressure distribution of the centrifugal pump impeller with splitter blades are more uniform, which increases the pump head by 10% to 15%. Gölcü M. [7–9] analyzed the influence of splitter blades on the performance of deep well centrifugal pumps. The results show that the use of splitter blades can effectively reduce energy consumption.

Shigemitsu T. et al. [10,11] improved the design of a small centrifugal pump in the form of adding splitter blades. It was found that the flow near the impeller outlet became uniform after the splitter blades were used, while the efficiency of the volute increased and the vortex loss decreased.

Yuan [12–14] discussed the principle and results of adding splitter blades based on the real flow in centrifugal pumps, the analysis results indicated that the splitter blades that deviated toward the suction surface of ordinary blades improved pump head and efficiency, adding splitter blades in the impeller moved the high efficiency point of the pump to the direction of large flow rate, and adding splitter blades in a screw-type centrifugal pump could decrease the radial forces on the impeller, but also decrease oscillations in volute as well. The influence of blade number was not considered in the analysis.

Zhang [15,16] investigated the influences of different positions of splitter blades on the performance of a centrifugal pump, two different splitter blade schemes were proposed: One located in the middle of the channel and the other having a deviation angle to the suction side of the long blade. The results showed that adding splitter blades can improve the tangential component distribution of absolute velocity at impeller outlet, and the streamline has a better consistency with the blades shape when splitter blades deviated to the long blade, which decreases energy loss.

Gu [17] and Cui [18] studied the effects of splitter blades on the performance and internal flow of low specific speed centrifugal pumps. Gu [17] found that both the vorticity and energy loss were enlarged around the volute tongue significantly after the blades passed by the cutwater, and the splitter blades produced more energy dissipation and unsteadiness than main blades. Cui [18] found that, at the design flow rate condition, both the efficiency and the head of the impeller with eight long blades were higher than those of the impeller with four long blades plus four splitter blades. While Cui [18] did not analyze the influence of deflection angle of splitter blades and bias angle in peripheral direction of splitter blades in the impeller optimization

Guo [19], Yuan [20] analyzed the influence of splitter blades on the internal pressure fluctuation and flow field of high-speed centrifugal pumps. Guo [19] clearly elucidated the anti-cavitation performance and the mechanism of bubble evolution of the high-speed centrifugal pump with splitter blades. Yuan [20] found that splitter blades obviously harmonized the turbulence kinetic energy distribution, and the pressure fluctuations distributed more evenly in the impeller, which enhanced the steady flow in the high-speed pump.

Jia et al. [21] carried out experiments to analyze the effect of the splitter blades on performance characteristics of a Francis turbine, and the results obtained were compared with those with normal blades. The results revealed that splitter blades increased the efficiency by approximately 2%, and they reduced the pressure fluctuation in the vaneless area under high-head operating conditions.

Although scholars around the world have carried out extensive and in-depth research on the splitter blades of ordinary centrifugal pumps, there is little research on the splitter blades of ultra-low specific speed magnetic driven centrifugal pumps. Based on the impeller of the prototype pump and the method of orthogonal test, nine different impellers are proposed in this paper. Blades number Z, bias angle in peripheral direction of splitter blades θ_s, inlet diameter of splitter blades D_{si}, and deflection angle of splitter blades α are selected as the main factors in the orthogonal test. Through the combination of numerical simulation and experiment, the influence of splitter blades on the performance of the ultra-low specific speed magnetic driven centrifugal pump is studied. The optimized impellers and the original impeller are analyzed and compared from internal flow field, pressure fluctuation, and radial force.

2. Materials and Methods

2.1. Orthogonal Test Design

The basic parameters of the magnetic drive pump for special engineering are as follows: Design flow rate Q_d is 8 $m^3 \cdot h^{-1}$, rated head H_d is 70 m, rotational speed n is 2900 $r \cdot min^{-1}$, specific speed n_s is

21, transmission medium is ethylene glycol aqueous solution, and temperature is normal. The main hydraulic dimensions of the impeller are as follows: Impeller outer diameter D_2 is 230 mm, outlet width b_2 = 5.2 mm, inlet diameter D_j is 40 mm, blade inlet placement angle is 24°, and outlet placement angle is 34°. Four long blades and four short blades are evenly distributed in the impeller. The inlet diameter of the splitter blades is 150 mm. The impeller and the internal magnetic rotor are integrated.

As the heart of the magnetic drive pump, the impeller is used to increase the pressure energy of the liquid. Different design parameters of splitter blades affect the performance of pump. According to previous research results, it is considered that the geometric parameters of splitter blades that affect the performance of magnetic drive pump are: The bias angle in peripheral direction of splitter blades θ_s, the inlet diameter of splitter blades D_{si}, the deflection angle of splitter blades α, and the blades number Z.

The increase of the number of blades has a great influence on the energy conversion of magnetic drive pump. The increase of the number of blades increases the finite blade correction coefficient, increases the head, and plays a decisive role in the performance change. Therefore, the number of blades Z was chosen as the first factor of orthogonal test.

The bias angle in the peripheral direction of splitter blades will affect the velocity distribution in the impeller passage, which will affect the performance of the magnetic drive pump. Therefore, the bias angle in the peripheral direction of splitter blades θ_s was chosen as the second factor of orthogonal test

The inlet diameter of splitter blades is related to the action length of splitter blades. Theoretically, the longer the splitter blades, the larger the head, so the inlet diameter D_{si} of splitter blades was selected as the third factor of the orthogonal test. The deflection angle of splitter blades α affects the velocity distribution of the impeller outlet, which has a significant influence on the performance of the magnetic drive pump. The deflection angle of splitter blades was selected as the fourth factor of the orthogonal test. Four selected factors of the orthogonal test are presented in Figure 1.

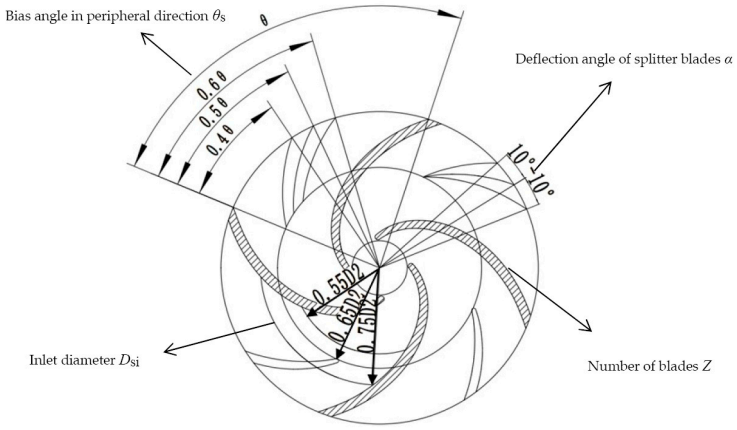

Figure 1. Schematic diagram of the four factors of the orthogonal test.

Table 1 lists three levels of the four factors in the orthogonal test. The factors of Z, θ_s, D_{si}, and α are expressed by code A, B, C, and D, respectively. Values of each factor are set within a certain range of the original impeller design value.

Table 1. Level table of the orthogonal test factors.

Levels	A	B	C	D
	Z	θ_s	D_{si}	α (°)
1	3	0.4θ	$0.55D_2$	−10
2	4	0.5θ	$0.65D_2$	0
3	5	0.6θ	$0.75D_2$	10

According to the selected four factors and three levels, the L_9 (3^4) orthogonal design schemes are established, as shown in Table 2.

Table 2. Orthogonal test schemes.

NO.	A	B	C	D	Parameter			
					Z	θ_s	D_{si}	α (°)
1	A_1	B_1	C_1	D_1	3	0.4θ	0.55 D_2	−10
2	A_1	B_2	C_2	D_2	3	0.5θ	0.65 D_2	0
3	A_1	B_3	C_3	D_3	3	0.6θ	0.75 D_2	10
4	A_2	B_1	C_2	D_3	4	0.4θ	0.65 D_2	10
5	A_2	B_2	C_3	D_1	4	0.5θ	0.75 D_2	−10
6	A_2	B_3	C_1	D_2	4	0.6θ	0.55 D_2	0
7	A_3	B_1	C_3	D_2	5	0.4θ	0.75 D_2	0
8	A_3	B_2	C_1	D_3	5	0.5θ	0.55 D_2	10
9	A_3	B_3	C_2	D_1	5	0.6θ	0.65 D_2	−10

According to orthogonal test schemes, the three-dimensional geometric models of nine impellers were constructed with UG NX9.0. Figure 2 shows water bodies of nine impellers.

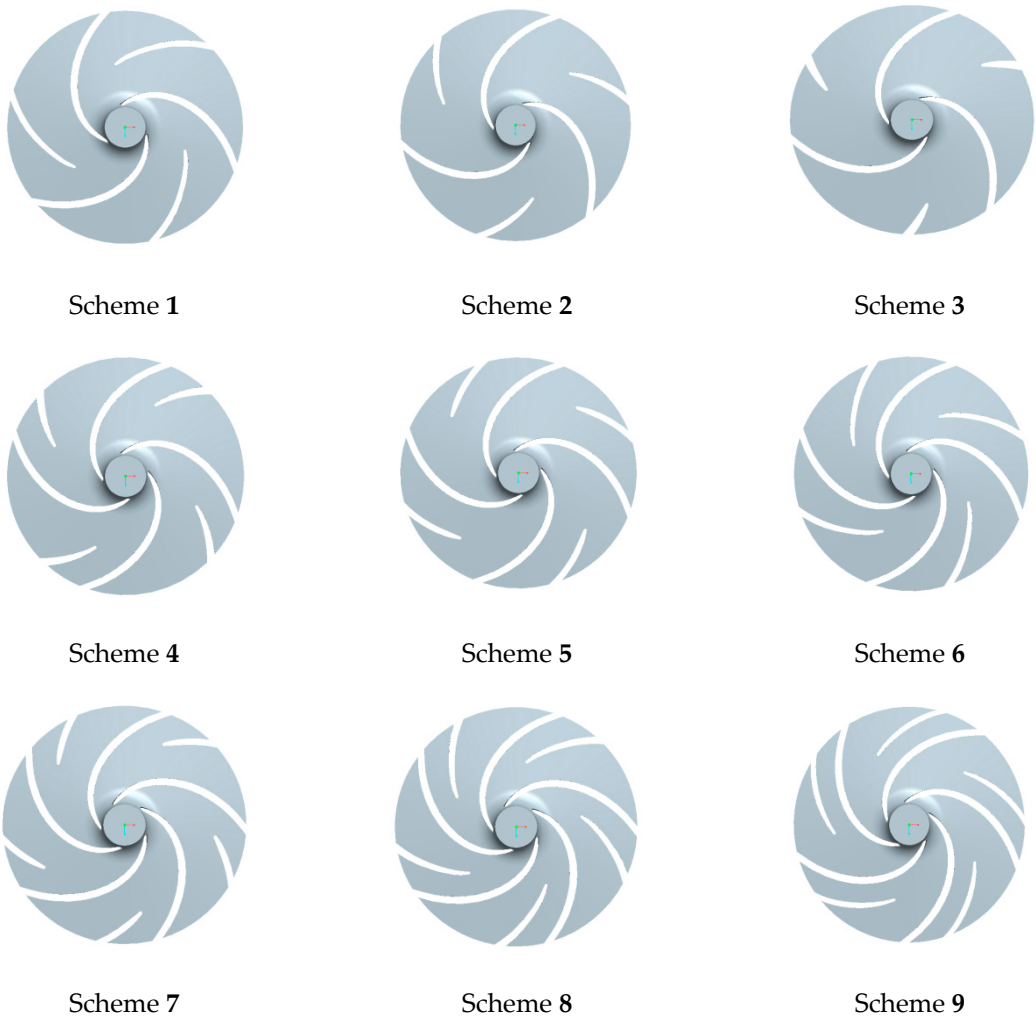

Figure 2. Water bodies of impellers corresponding to orthogonal test schemes.

2.2. Calculation Model

The compact magnetic drive pump features a direct-connected construction. The impeller and the inner magnet are integral and are rotating parts. The pump shaft and the isolation sleeve are integrated and are stationary parts. The structure ensures that the magnetic drive pump has a small size, light weight, no leakage, and reliable operation. The configuration of the magnetic drive pump is shown in Figure 3.

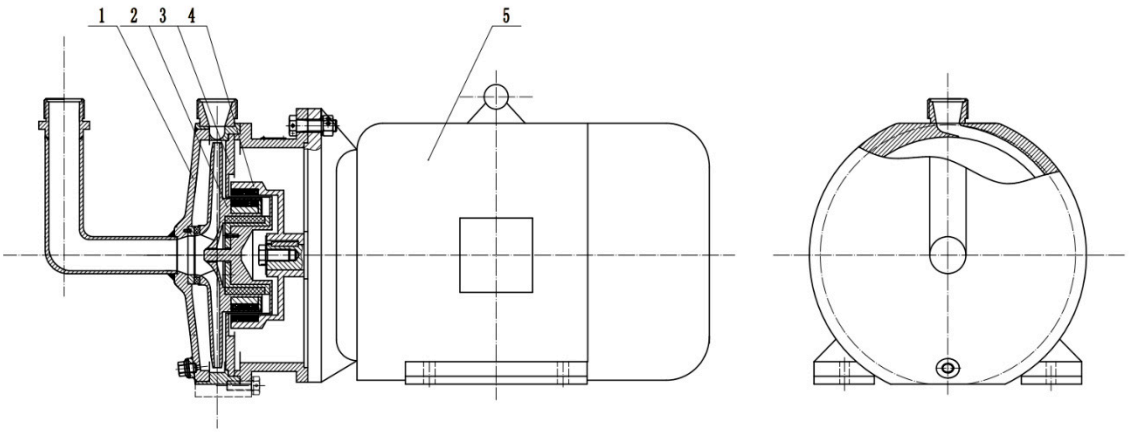

Figure 3. Configuration of the magnetic drive pump. 1—pump shell; 2—impeller; 3—isolation sleeve; 4—external magnetic rotor; 5—motor.

The computational domain of the whole flow field mainly includes the inlet pipe fluid, the impeller internal fluid, the pump internal fluid, the cooling circulating fluid in the pump, and the outlet pipe fluid. As shown in Figure 4, the inlet and outlet sections were extended appropriately in order to obtain stable inlet and outlet flow.

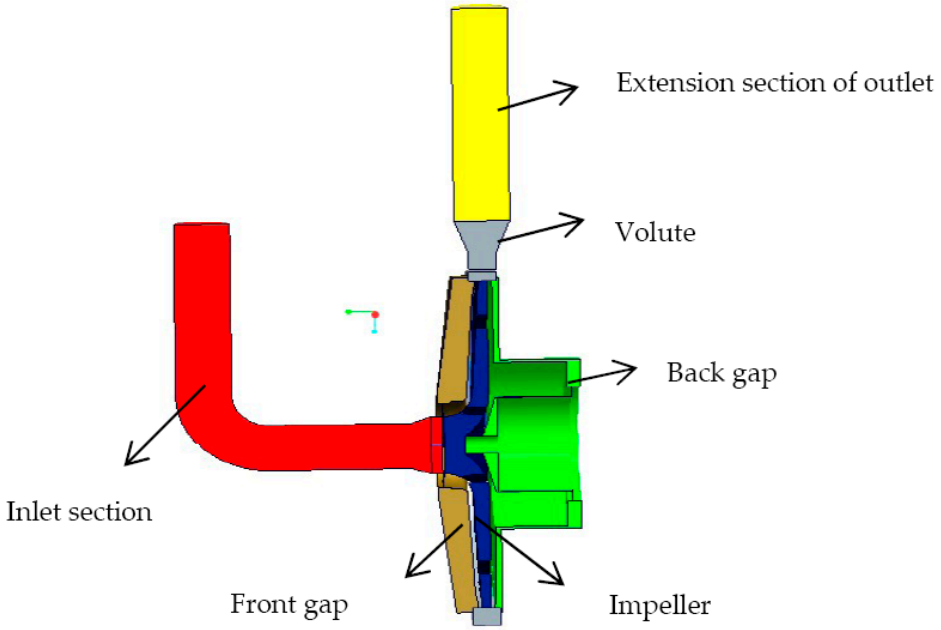

Figure 4. Calculation domain of magnetic drive pump flow field.

2.3. Mesh Generation and Independence Verification

Hexahedral structured meshes were generated in the flow field by ANSYS-ICEM 14.5 (ANSYS, Inc., Canonsburg, PA, USA). Meshes in the impeller blade wall were refined. The meshes of magnetic

drive pump are shown in Figure 5. In order to reduce the computational load and ensure the accuracy of numerical calculation results, mesh independence analysis was carried out. Four groups of meshes with different numbers were divided, and ANSYS-CFX 14.5 (ANSYS, Inc., Canonsburg, PA, USA) was used to simulate the performance at design flow rate condition. The head and efficiency were selected as evaluation indicators. Mesh independence analysis is shown in Table 3. When the total number of grids is greater than 1,254,650, the head and efficiency of the magnetic drive pump change little, so 1,254,650 is chosen as the number of grids for numerical simulation.

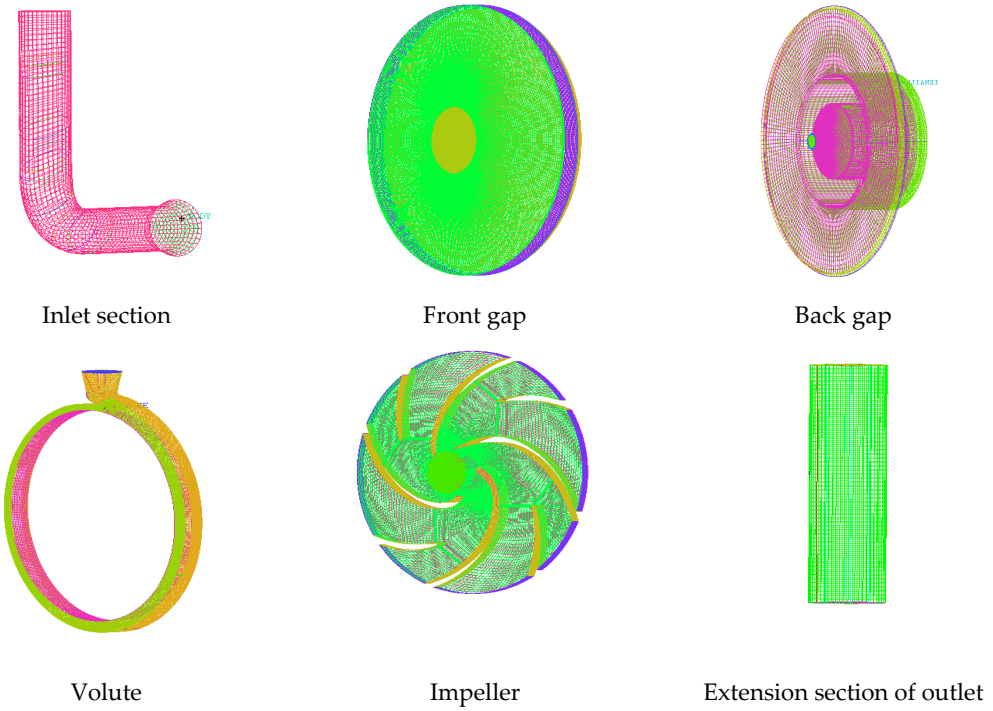

(**a**) Mesh of major hydraulic components

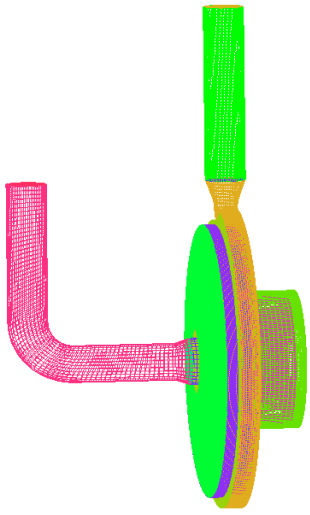

(**b**) Mesh assembly

Figure 5. Field mesh of the magnetic drive pump.

Table 3. Mesh independence analysis.

Number of Grids	Head (m)	Efficiency
575,681	77.84	0.3865
960,887	78.48	0.3929
1,254,650	78.94	0.4067
1,638,560	78.98	0.4065

2.4. Turbulence Model

In actual engineering, all flow problems should satisfy the laws of conservation of mass, momentum, and energy. The fluid flow studied in this paper is a three-dimensional incompressible turbulent flow. The turbulence model selected for numerical simulation is the SST (Shear Stress Transport) $k-\omega$ model, which is a mixture of model $k-\varepsilon$ and model $k-\omega$. It not only has the reliability of the model $k-\omega$ in calculating the viscous flow in the near-wall region, but also has the accuracy of the model $k-\varepsilon$ in calculating the free flow of the far-field head [22]. The basic governing equations of the SST $k-\omega$ model are as follows [23,24]:

$$\frac{\partial(\rho k)}{\partial t}+\frac{\partial}{\partial x_i}(\rho u_i k)=\frac{\partial}{\partial x_i}\left[\left(\mu+\frac{\mu_i}{\sigma_k}\right)\frac{\partial k}{\partial x_i}\right]+P_k-\beta'\rho k\omega \tag{1}$$

$$\frac{\partial(\rho\omega)}{\partial t}+\frac{\partial}{\partial x_i}(\rho u_i \omega)=\frac{\partial}{\partial x_i}\left[\left(\mu+\frac{\mu_i}{\sigma_k}\right)\frac{\partial \omega}{\partial x_i}\right]+D_m+\alpha\frac{\omega}{k}P_k-\beta\rho\omega^2 \tag{2}$$

where $\beta' = 0.09$, $\alpha = 5/9$, $\beta = 0.075$ and $\sigma_k = 2$, ρ stands for density (kg·m^{-3}), P_k represents turbulent productivity [25,26].

2.5. Steady Computation Settings

The assembly mesh of computational domain was imported in ANSYS-CFX and calculation type was defined as a constant calculation. The magnetic drive pump impeller was set to the rotation domain, and the other calculation fields were set to the stationary calculation domain.

The import boundary definition was set on the inlet face of the inlet section, and the boundary condition type was set to the static pressure inlet. The pressure was set to a standard atmospheric pressure and the turbulence intensity was chosen to be 5%, corresponding to the moderate turbulence. The exit boundary was defined on the exit face of the outlet extension and the boundary condition type was set to the mass flow outlet.

The interface between the impeller rotation domain and other calculation domains was set to the dynamic–static calculation domain interface, the type was set to frozen rotor type, and the other interfaces were set to the static–static calculation domain interface.

The impeller speed of the magnetic drive pump was set to 2900 r/min. According to the actual temperature of the medium delivered in the pump, the simulated medium was water and the water temperature was set to 25 °C. The wall condition was set to a non-slip solid wall condition, and the wall roughness was set to 15 μm (equivalent value of surface roughness in pump cavity). The time item for solving the parameter was set to the automatic time step and the residual convergence value was set to 10^{-5}.

2.6. Test Bench for Magnetic Drive Pump

The prototype pump experiment was carried out at the special pump test bench in the National Pump Engineering Technology Research Center of Jiangsu University. Schematic diagram of the magnetic drive pump test bench structure is shown in Figure 6, and Figure 7 is the scene of magnetic drive pump experiment.

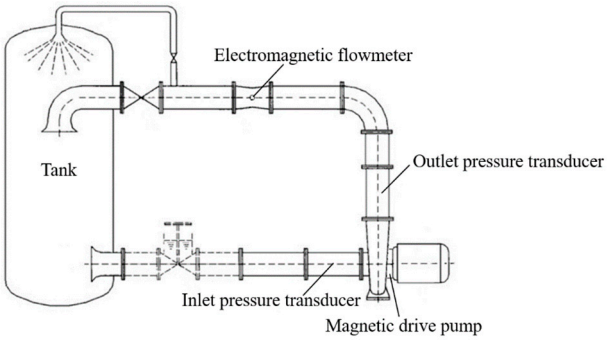

Figure 6. Magnetic drive pump test bench structure.

Figure 7. Drive pump test bench.

OPTIFLUX 2100 electromagnetic flowmeter was used in the magnetic drive pump test bench to realize the instantaneous measurement of flow. Its measurement range is 0 to 30 $m^3 \cdot h^{-1}$, the measurement accuracy is less than 0.5%, and the uncertainty of the flow measurement is ±0.2%. The WIKA S10 pressure transmitter is used to measure the instantaneous pressure at the inlet and outlet of the pump. The range of the pressure transducer at the inlet and outlet of the pump is −1 to 1 MPa and 0 to 1.6 MPa, respectively. Its measurement accuracy is less than 0.25%, and the uncertainty of the pressure measurement is ±0.1%.

The output signals of flow and pressure sensors are 4–20 mA current signals, which are collected by high-speed data acquisition card and stored in PC for data processing.

3. Results and Discussion

3.1. Experimental Verification

To verify the reliability of the numerical calculation, the numerical calculation results at different flow rate conditions were compared with the experimental data of the magnetic drive pump prototype. The external characteristic curves drawn by the experimental data at different flow rate conditions were compared with the ANSYS-CFX numerical simulation results, as shown in Figure 8.

From the flow-head curve, it can be seen that the simulation calculation agrees well with the experiment near the design flow rate condition, and there are slight deviations between the numerical calculation and the experimental results under other flow rate conditions. The reason for the deviation may be that the stability of the flow field is poor and the boundary layer is separated under non-rated conditions. In this condition, if numerical simulation still uses the steady flow model, the error would occur. The simulation efficiency agrees well with the experiment efficiency near the design flow rate

condition. In the flow rate range of 0.6 and 1.4 Q_d, the maximum relative error of efficiency is 4.4% (at 0.6 Q_d). In conclusion, the general trends of the simulation and experiment results are consistent, and the numerical simulation results of the whole flow field in the magnetic drive pump are true and credible.

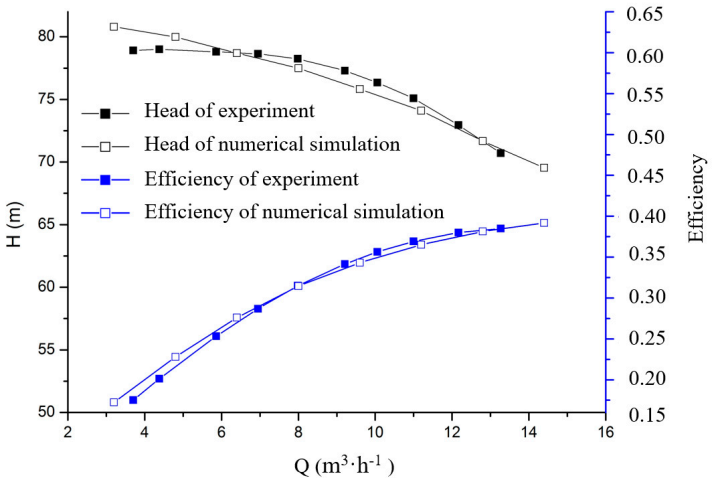

Figure 8. Characteristic curve of numerical simulation and prototype experiment.

3.2. Internal Flow Analysis of Impeller

The internal flow condition of the impeller reflects the advantages and disadvantages of the hydraulic design. The nine impeller schemes were numerically simulated, respectively, and the internal flow cloud diagram of the impellers at design flow rate condition are shown in Figure 9.

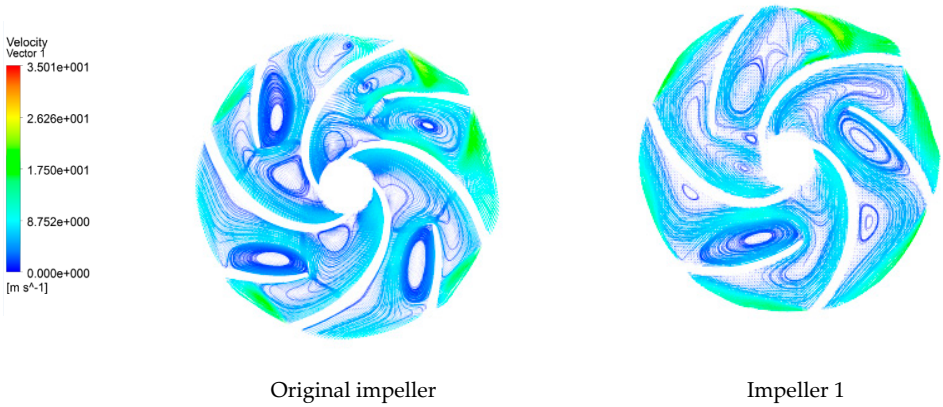

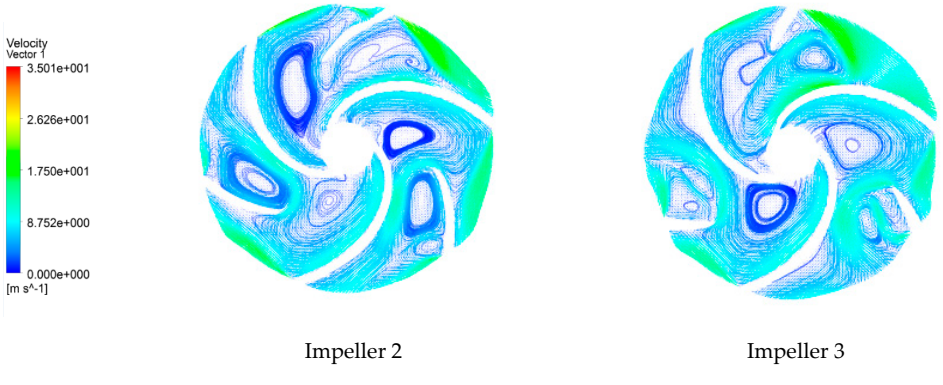

Figure 9. *Cont.*

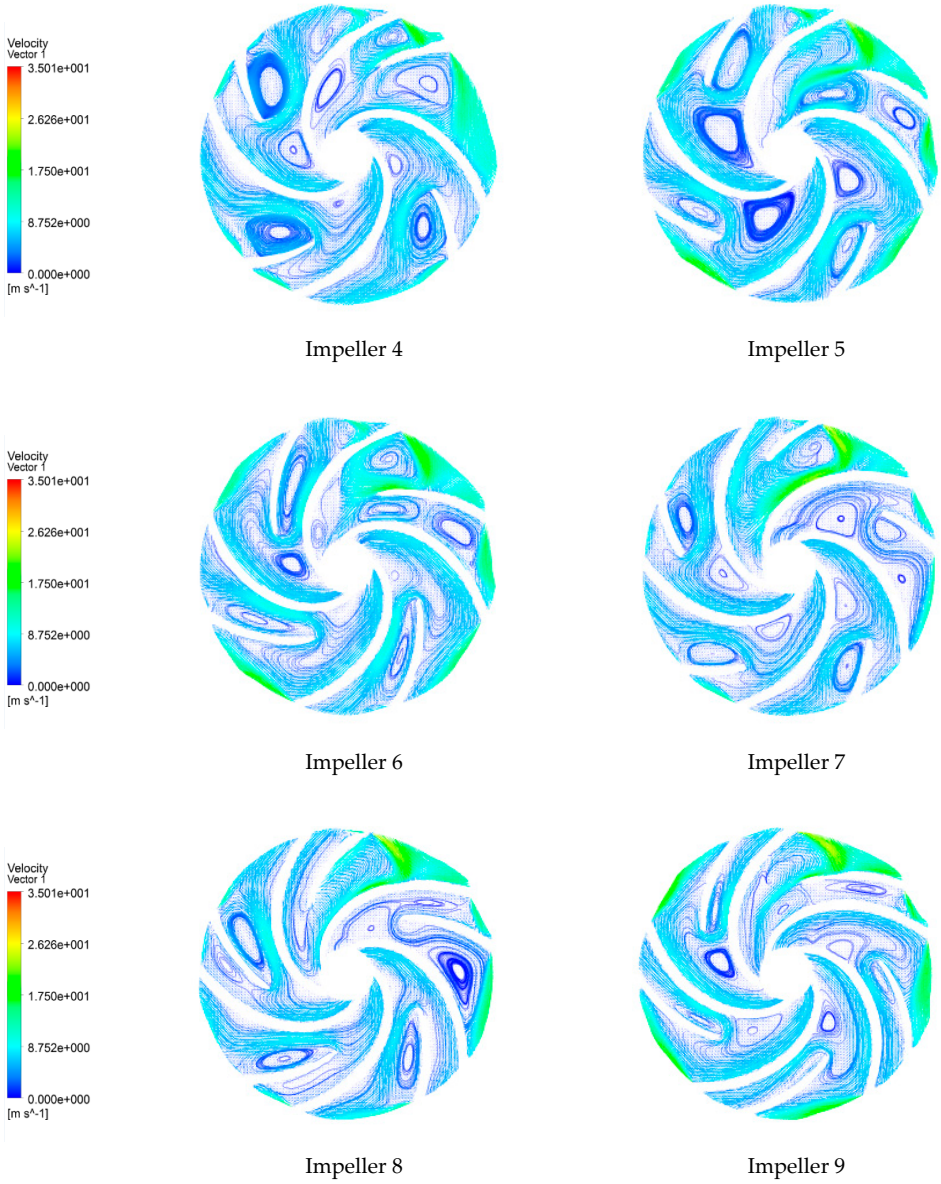

Figure 9. Flow cloud diagram of the nine impellers at design flow rate condition.

From Figure 9, it can be seen that, due to the low specific speed of the compact magnetic drive pump and the narrow inner passage of the impeller, there are vortices in the impeller of all schemes. Schemes 1–3 have larger low-speed vortices and larger high-speed flow areas at the outlet of impellers, resulting in worse internal flow conditions. Schemes 4–6 are similar to the internal flow condition of the original design. Vortexes appeared on the back of the splitter blade and inside the working face of the main blade, and the flow is not uniform. The internal flow of the impellers in Schemes 7–9 is more uniform than that of other schemes, and there are less internal vortices. The flow condition in the flow passage is better improved with the increase of the blades, and the energy loss is reduced. The flow condition of Scheme 7 is optimal in all schemes, with the least impeller exit wake region and vortex.

3.3. Range and Variance Analysis of Performance Indexes

The efficiency and head of each scheme impeller obtained by numerical simulation are shown in Table 4, in which scheme 0 corresponds to the original design impeller.

Table 4. Efficiency and head of different scheme.

Scheme Number	Head (m)	Efficiency
0	77.98	0.4212
1	71.23	0.4368
2	72.78	0.4215
3	74.41	0.3743
4	76.57	0.4129
5	77.03	0.4156
6	77.75	0.4076
7	80.07	0.4415
8	77.67	0.4429
9	75.62	0.4446

The range analysis of head and efficiency was conducted based on the orthogonal test results in Table 5. In Table 5, H represents the performance index of head (m), η represents the performance index of efficiency in percentage, K represents the sum of the test results at the corresponding level, k represents the average value of the test results at the corresponding level, and R represents the range value of k.

Table 5. Range analysis of head and efficiency.

		Factor						Factor		
		A	B	C	D		A	B	C	D
Index		Z	θ_s	D_{si}	α	Index	Z	θ_s	D_{si}	α
H	K_1	218.42	227.87	226.65	223.88	η	K_1	123.26	129.12	128.73	129.7
	K_2	231.35	227.48	224.97	230.6		K_2	123.61	128	127.9	127.06
	K_3	233.36	227.78	231.51	228.65		K_3	132.9	122.65	123.14	123.01
	k_1	72.81	75.96	75.55	74.63		k_1	41.09	43.04	42.91	42.23
	k_2	77.12	75.83	74.99	76.87		k_2	41.20	42.67	42.63	42.35
	k_3	77.78	75.93	77.17	76.22		k_3	44.3	40.88	41.05	41.00
	R_H	4.97	0.13	2.18	2.24		R_η	3.21	2.16	1.86	1.35

According to the principle of the orthogonal test, the influence of the factors on the result is directly proportional to the magnitude of the range. Therefore, the sequence of factors affecting the head of the magnetic drive pump is ADCB, namely, blades number, deflection angle, inlet diameter of splitter blades, and bias angle in the peripheral direction. The sequence of factors affecting the efficiency of the magnetic drive pump is ABCD, namely, blades number, bias angle in the peripheral direction, inlet diameter of splitter blades, and deflection angle. The effects of various factors on head and efficiency are shown in Figures 10 and 11, respectively.

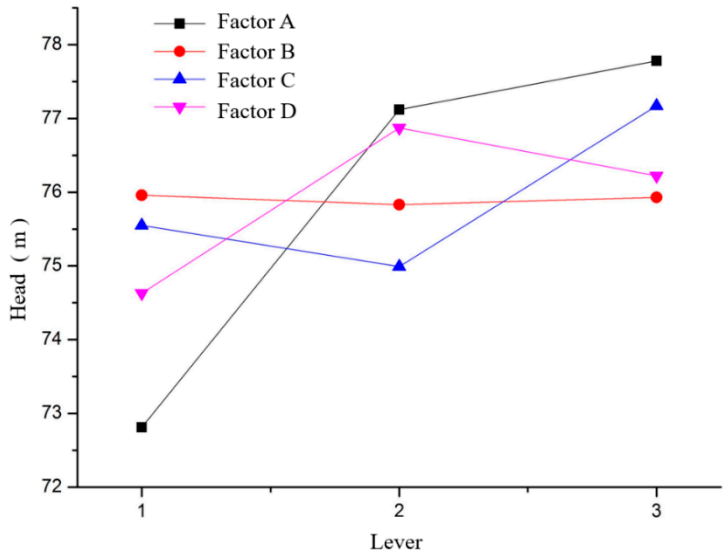

Figure 10. Curve.

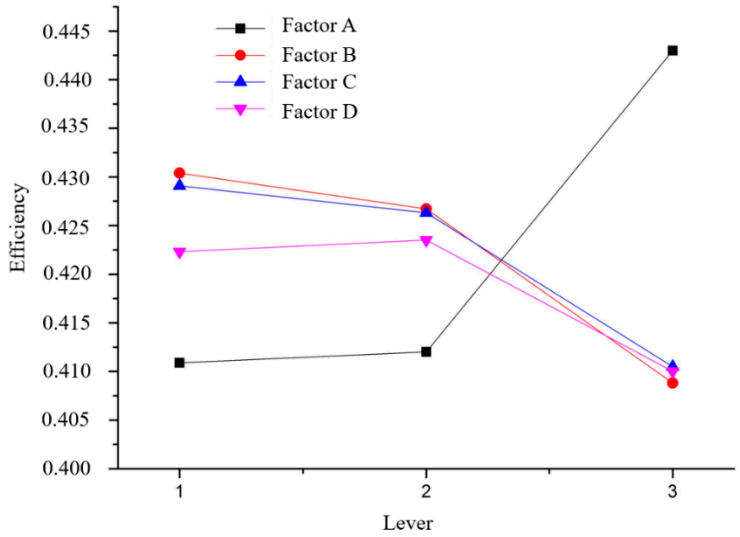

Figure 11. Curve.

The influence of each factor level on the performance of the magnetic drive pump is as follows:

(1) For factor A, the head increases with the increase of the number of blades. The head increases sharply from A_1 to A_2, while the head increases slowly from A_2 to A_3. The head reaches the maximum at A_3. The efficiency increases with the increase of the number of blades. Efficiency increases slowly from A_1 to A_2, while the efficiency curve increases sharply from A_2 to A_3. The efficiency at A_3 is the highest. Considering the influence of factor level on head and efficiency, A_3 (the number of blades Z = 5) is the best choice.

(2) For factor B, the change of bias angle in the peripheral direction has no obvious effect on head. The efficiency decreases gradually with the increase of bias angle in the peripheral direction. The efficiency reaches the highest when the bias angle is $0.4\theta(B_1)$. Therefore, it is reasonable to select the bias angle of 0.4θ.

(3) For factor C, the head is the highest at C_3 (the inlet diameter of splitter blades $D_{si} = 0.75D_2$), while the efficiency is the lowest at C_3. The head at C_1 (the inlet diameter of splitter blades $D_{si} = 0.55D_2$) is slightly lower than that at C_3, while the efficiency at C_1 is the highest. If more consideration

is given to head, C_1 is chosen. If the head at C_1 and C_3 has met the design requirements, C_3 is more energy-saving.

(4) For factor D, the variation trend of the head curve and efficiency curve is basically the same. When the deflection angle of splitter blades is 0° (D_2), the head and efficiency both reaches the maximum; therefore, the best deflection angle was 0°.

The Taguchi method and ANOVA (Analysis of Variance) were applied to find the proportion of the influence of each orthogonal factor on the performance indexes. The Taguchi method is an optimal design method based on the orthogonal test, which was proposed by Dr. Taguchi of Japan. The Taguchi method can optimize the design of multiple objectives. Through the establishment of the orthogonal test table and the ANOVA of the orthogonal test results, the best combination of design parameters can be obtained with the least number of tests [27,28]. Analysis of variance of factors is conducted based on orthogonal test results (Tables 4 and 5), and the analysis results are given in Table 6.

Table 6. Variance of each factor and percentage of influence on performance indexes.

Factors	Head		Efficiency	
	Variance Value	Influence Ratio (%)	Variance Value	Influence Ratio (%)
A (Z)	4.857	73.602	2.214	51.972
B (θ_s)	0.003	0.046	0.890	20.892
C (D_{si})	0.854	12.941	0.670	15.728
D (α)	0.885	13.411	0.486	11.408
Sum	6.599	100	4.26	100

As can be seen in Table 6, factor A (73.602%) has the decisive influence on head. Factor D (13.411%) and factor C (12.941%) influence the head greatly, while factor B (0.046%) has the least influence on the head.

The results of variance analysis show that the influence proportion of each factor on efficiency are: Factor A (51.972%), factor B (20.892%), factor C (15.728%), and factor D (11.408%), respectively.

Factor A has a greater influence on both head and efficiency than other factors. For factor C, the influence ratio on efficiency (15.728%) is higher than the influence on head (12.941%).

Based on the Taguchi method, combined with the data in Tables 5 and 6, two sets of optimized impeller combinations are obtained. The combination of $A_3B_1C_3D_2$ has the best head, while the combination of $A_3B_1C_1D_2$ has the best efficiency. Table 7 lists the parameters of the two optimized impellers.

Table 7. Parameters of the two optimized impellers.

Combination	Parameter			
	Z	θ_s	D_{si}	α (°)
$A_3B_1C_3D_2$	5	0.4 θ	0.75 D_2	0
$A_3B_1C_1D_2$	5	0.4 θ	0.55 D_2	0

The above analysis shows that the better design schemes of split blades is $A_3B_1C_3D_2$ and $A_3B_1C_1D_2$. $A_3B_1C_3D_2$ is Scheme 7 of the orthogonal test. The combination scheme of $A_3B_1C_1D_2$ did not appeared in the test schemes, and is newly named as Scheme 10. Modeling and numerical simulation of Scheme 10 was conducted. Figure 12 is the water body model of the impeller of Scheme 10, and Figure 13 is its inner flow cloud diagram. It could be seen that the inner vortex of the impeller of Scheme 10 is less and the streamline is more stable than that of Scheme 7 (shown in Figure 9).

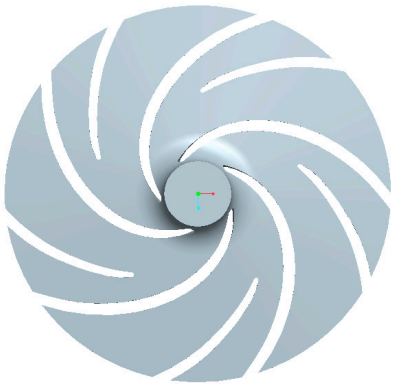

Figure 12. Model of impeller 10.

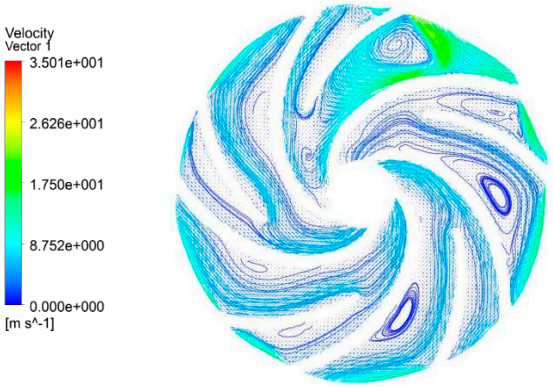

Figure 13. Flow cloud diagram of impeller 10.

Comparisons of impeller performance between Scheme 7 ($Z = 5$, $\theta_s = 0.4\theta$, $D_{si} = 0.75D_2$, $\alpha = 0°$) and Scheme 10 ($Z = 5$, $\theta_s = 0.4\theta$, $D_{si} = 0.55D_2$, $\alpha = 0°$) is shown in Figure 14. The head of Scheme 10 is 77.12 m, which is lower than that of Scheme 7 (80.07 m). The efficiency of Scheme 10 is 45.59%, which is higher than that of Scheme 7 (44.15%). Scheme 7 increases the head and efficiency by 2.68% and 4.82%, respectively. Scheme 10 reduces the head by 0.33% and increases the efficiency by 8.24%. The data shows that the decrease of inlet diameter of splitter blades improves the flow condition inside the impeller, reduces the energy loss, and improves the efficiency.

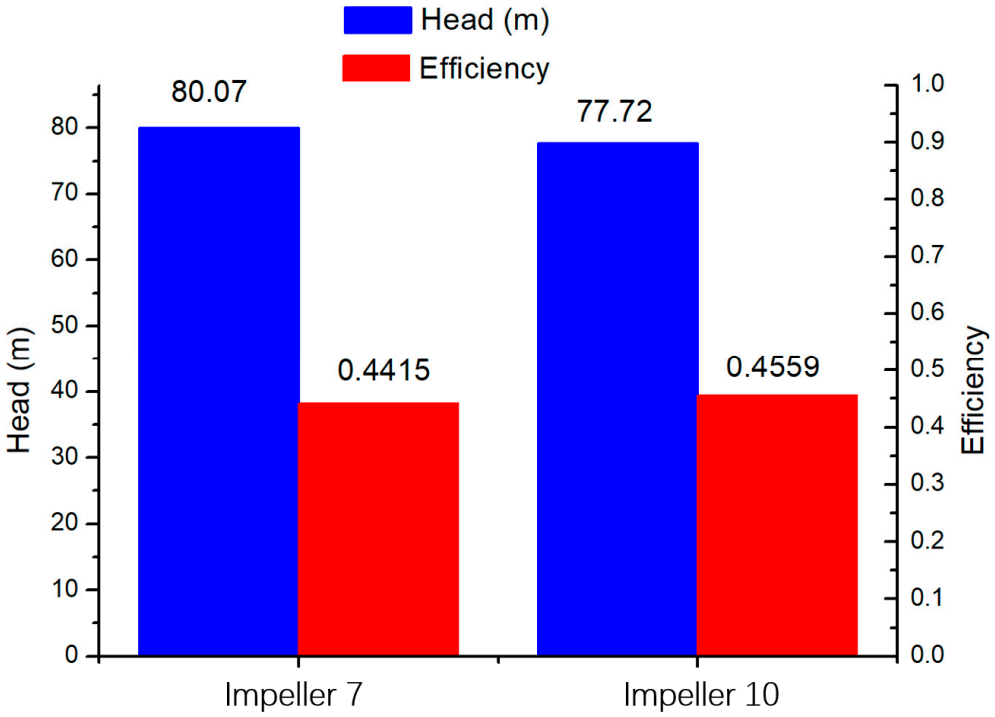

Figure 14. Performance comparison of impeller 7 and impeller 10.

3.4. Analysis of Pressure Fluctuation

Pressure fluctuation is the main factor affecting the stable operation of the pump. The transient numerical calculation of the whole flow field of the magnetic drive pump was carried out. A pressure fluctuation monitoring point was set at the volute tongue. The location of the monitoring point is shown in Figure 15. The steady calculation results were taken as the initial condition of transient calculation. Because the rated speed of the impeller is 2900 r/min, considering the economy of calculation, the final time step was 1.7241×10^{-4} s, namely, the impeller rotated 3° per time step.

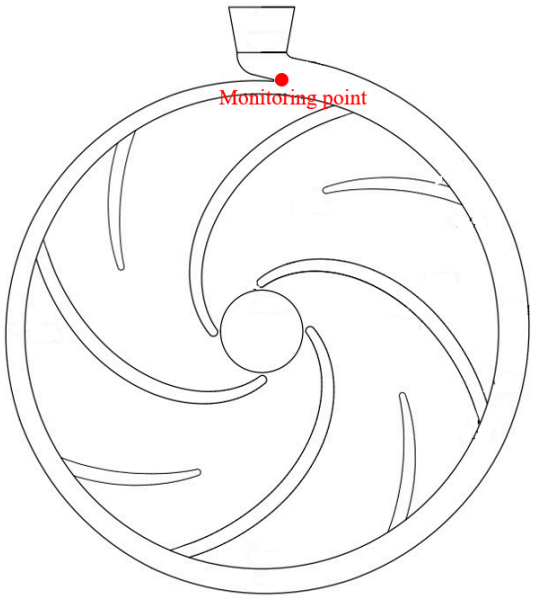

Figure 15. Location of monitoring point.

The pressure fluctuation of the original impeller, impeller 7, and impeller 10 at different flow rate conditions (0.6 Q_d, 1.0 Q_d and 1.5 Q_d) in one period is presented in Figure 16. It can be seen from Figure 16 that the instantaneous low pressure appears in the original impeller, and the pressure fluctuation of the original impeller is the most disordered. The peak-to-peak values of pressure fluctuation of impellers 7 and 10 are smaller than those of the original impeller.

At small flow rate condition (0.6 Q_d), the pressure fluctuation amplitudes of the three impellers are close. The pressure fluctuation of impellers 7 and 10 are more stable than those of the original impeller at design and large flow rate conditions, and the average pressure values of impellers 7 and 10 are higher than those of the original impeller. The pressures of impellers 7 and 10 are higher than those of the original impeller, which bring higher heads to the magnetic drive pump.

Comparing the pressure fluctuation of impellers 7 and 10 further, the peak-to-peak value of impeller 10 is slightly smaller than that of impeller 7 at small flow rate condition (0.6 Q_d), and the pressure fluctuation performance of impeller 10 is more stable. At design flow rate condition (1.0 Q_d), the average pressure amplitude of impeller 10 is slightly smaller than that of impeller 7, which is consistent with the conclusion of the higher head of impeller 7 mentioned above. At large flow rate condition (1.5 Q_d), the pressure fluctuation of impeller 7 is the most consistent with that of impeller 10, and the fluctuation amplitude, maximum peak value, and minimum peak value are close to each other.

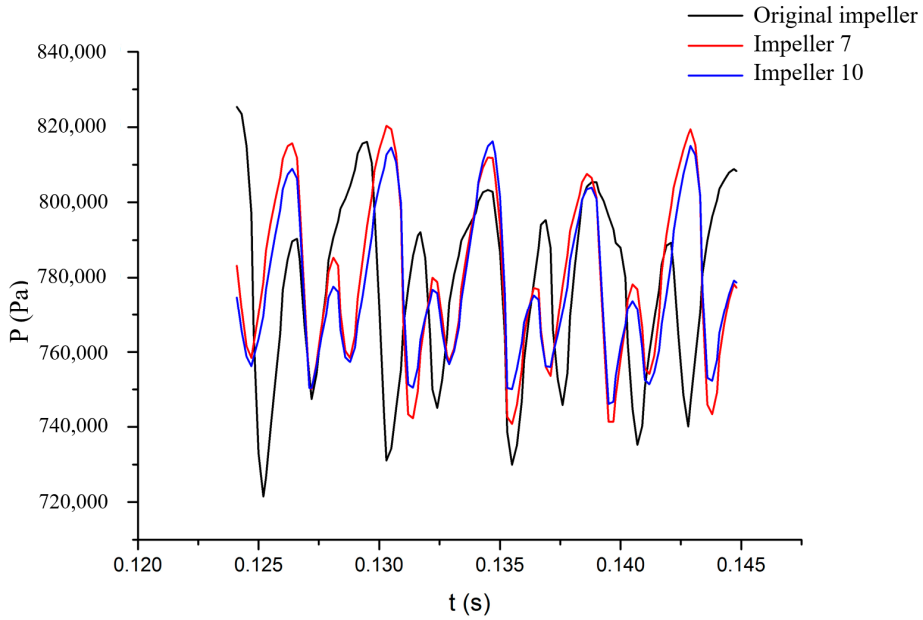

(**a**) 0.6 Q_d

Figure 16. *Cont.*

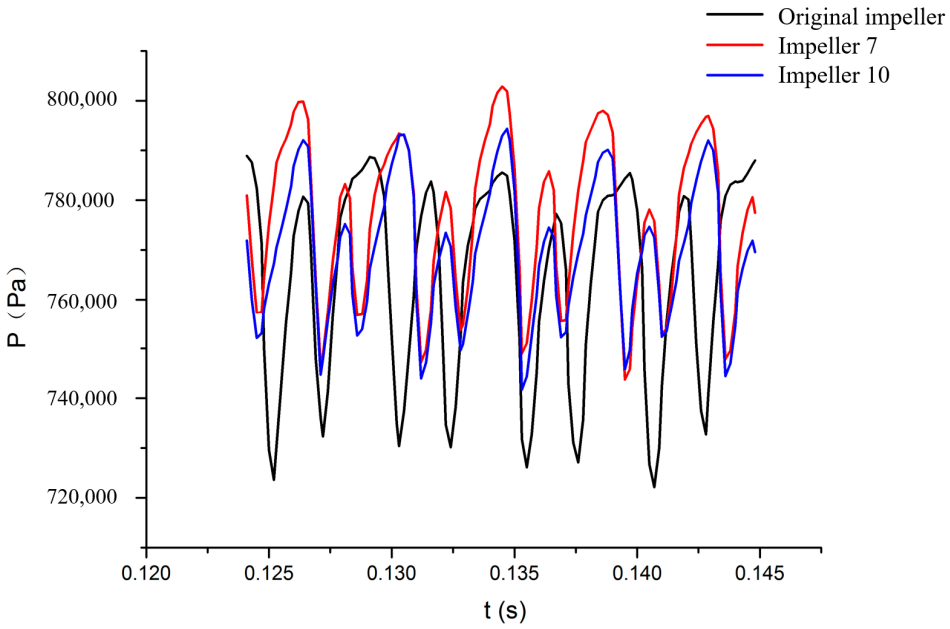

(**b**) 1.0 Q_d

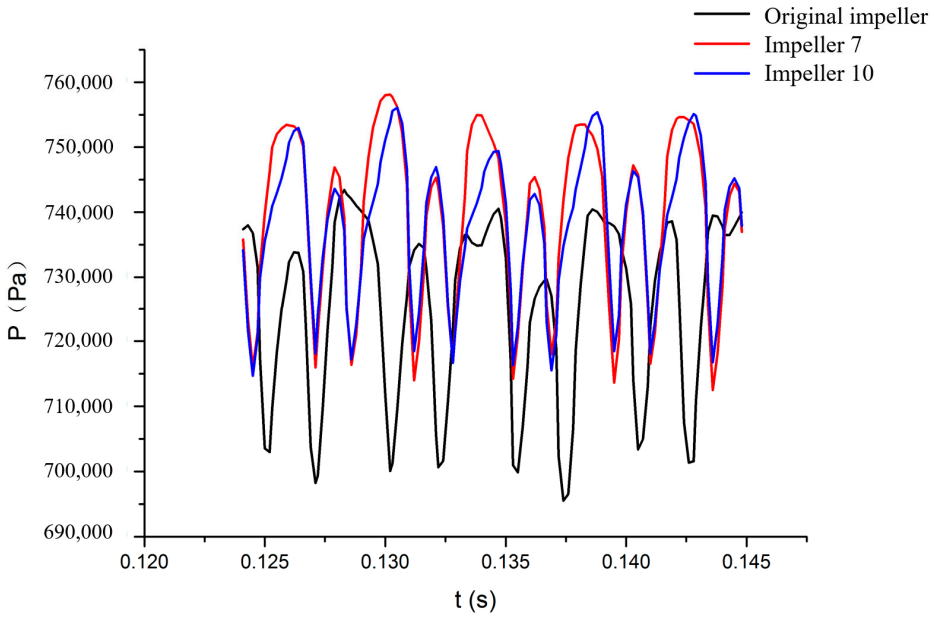

(**c**) 1.5 Q_d

Figure 16. Comparison of pressure fluctuation of different impellers.

3.5. Analysis of Radial Force

The radial forces of the original impeller, impeller 7, and impeller 10 at different flow rate conditions are shown in Figure 17. It can be seen from the figure that the radial force amplitudes of the three impellers are similar at different flow rate conditions, and the radial force gradually decreases as the flow rate increases. By comparison, the radial force circumferential distribution of impeller 10 is the most uniform at each flow rate condition.

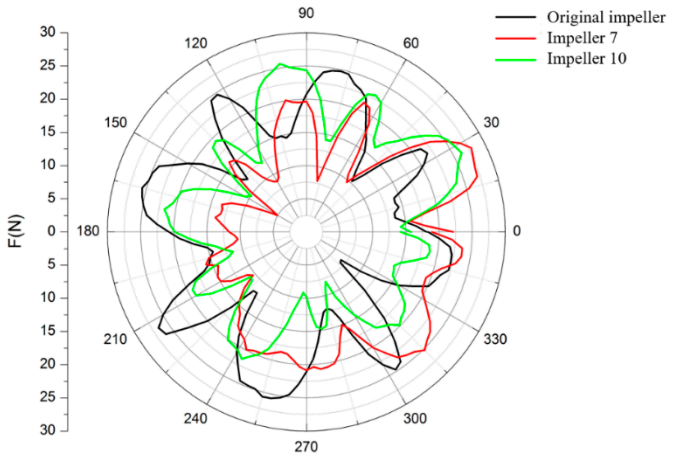

(**a**) 0.6 Q_d

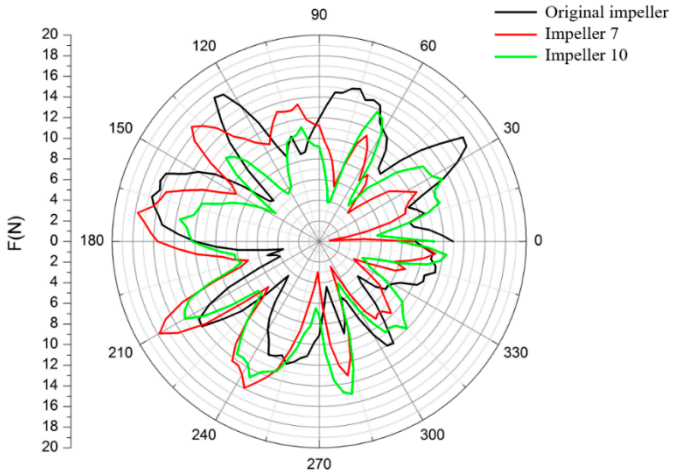

(**b**) 1.0 Q_d

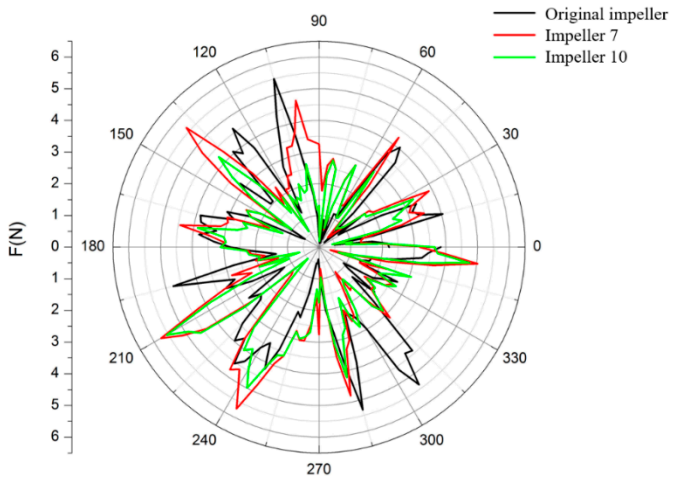

(**c**) 1.5 Q_d

Figure 17. Comparison of radial force of different impellers.

The variance analysis of the radial forces of different impellers was carried out. Figure 18 shows the variance histograms of the three impellers at different flow rate conditions. It could be seen from the figure that impeller 10 has the smallest variance and impeller 7 has the largest variance at different flow rate conditions, so the radial force distribution of impeller 10 is the most stable among the three impellers.

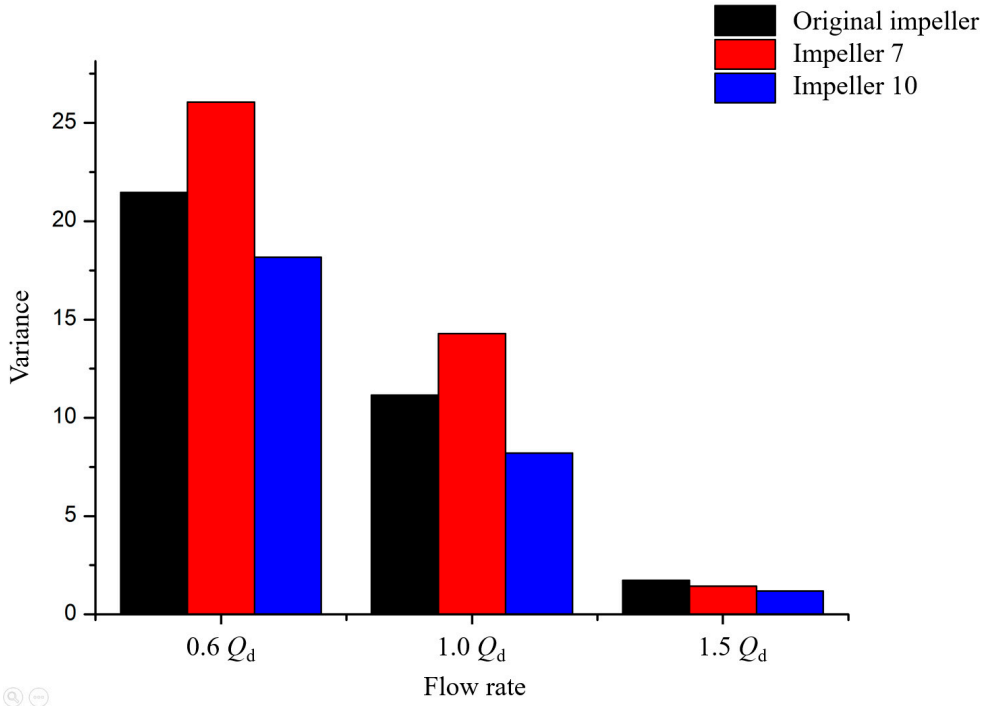

Figure 18. Diagram of radial force for different impellers.

4. Conclusions and Future Work

With the characteristics of electromagnetic transmission, no leakage, and compact structure, magnetic drive pumps are widely used in aerospace, chemical, pharmaceutical, and military industries. The efficiency of magnetic drive pumps is usually lower than that of ordinary mechanical seal pumps. To improve the performance of an ultra-low specific speed magnetic drive pump, combining numerical simulation with experiment, the optimized design of the impeller was carried out. The blades number Z, the bias angle in the peripheral direction of splitter blades θ_s, the inlet diameter of splitter blades D_{si}, and the deflection angle of splitter blades α were taken as the main factors in the orthogonal test, and two sets of better impeller design parameters were found. The optimized impellers and the original impeller were compared in internal flow, pressure fluctuation, and radial force. The accuracy of the numerical simulation was verified by prototype experiments. In the flow rate range of 0.6 Q_d and 1.4 Q_d, the maximum relative errors of head and efficiency were 2.1% and 4.4%, respectively. The main conclusions were drawn as follows:

(1) The factors affecting the head of magnetic drive pump in descending order were: Blades number, deflection angle, inlet diameter of splitter blades, and bias angle in the peripheral direction. The factors affecting efficiency in descending order were: Blades number, bias angle in the peripheral direction, inlet diameter of splitter blades, and deflection angle.

(2) Impeller 7 ($Z = 5$, $\theta_s = 0.4\theta$, $D_{si} = 0.75D_2$, $\alpha = 0°$) increased the head and efficiency by 2.68% and 4.82%, respectively. Impeller 10 ($Z = 5$, $\theta_s = 0.4\theta$, $D_{si} = 0.55D_2$, $\alpha = 0°$) reduced the head by 0.33% and increases the efficiency by 8.24%.

(3) At small flow rate condition (0.6 Q_d), the pressure fluctuation amplitudes of the three impellers were close. At design flow rate condition (1.0 Q_d) and large flow rate condition (1.5 Q_d), the pressure fluctuations of impeller 7 and impeller 10 were more stable than that of the original impeller, and the average pressure of each new impeller was higher than that of the original impeller, respectively.

(4) At flow rate conditions of 0.6, 1.0, and 1.5 Q_d, impeller 10 had the smallest radial force variance, and its radial force distribution was more stable than those of the original impeller and impeller 7.

This paper did not analyze the disk energy loss and axial force distribution of the optimized impellers. In the future, numerical simulation and experiments will be combined to further analyze the performance of optimized impellers. In addition, how to reduce the noise and vibration of the magnetic driven centrifugal pump is the next research direction.

Author Contributions: F.Z. and F.K. presented the optimal scheme and designed the experiments. F.Z. and Y.Z. made the numerical simulation and performed the experiment. F.Z., Y.B. and B.X. analyzed the data. F.Z. wrote the paper.

Funding: This research was funded by: the Priority Academic Program Development (PAPD) of Jiangsu Higher Education Institutions; the Industry-University-Research Cooperation Project of Jiangsu Province; the Excellent scientific and technological innovation team of Jiangsu Higher Education Institutions (Intelligent Manufacturing Equipment Design and Engineering Application); the National Natural Science Foundation of China, grant number 11602097; the Top-Notch Academic Programs Project of Jiangsu Higher Education Institutions, grant number PPZY2015A086; the Natural Science Foundation of the Jiangsu Higher Education Institutions of China, grant number 19KJD470006; and the Scientific Research Project of Wuxi Institute of Technology, grant number ZK201804.

Conflicts of Interest: The authors declare no conflicts of interest.

References

1. Brodersen, S. Magnetic-drive pumps: Technology and new applications. *Hydrocarb. Process.* **2001**, *80*, 45–48.
2. Thompson, K. What the future holds for magnetic drive pumps. *World Pumps.* **2007**, *495*, 28–29. [CrossRef]
3. Kong, F.Y.; Shen, X.K.; Wang, W.T.; Zhou, S.Q. Performance Study Based on Inner Flow Field Numerical Simulation of Magnetic Drive Pumps with Different Rotate Speeds. *Chin. J. Mech. Eng.* **2012**, *25*, 137–143. [CrossRef]
4. Borovsky, J.E.; Horne, R.B.; Meredith, N.P. The contribution of compressional magnetic drive pumping to the energization of the Earth's outer electron radiation belt during high-speed-stream-driven storms. *J. Geophys. Res. Sp. Phys.* **2017**, *122*, 12072–12089.
5. ХлопеНКоВ.п.р.; Zhuang, C.R. Translated. On the issues of the optimization of the structure of centrifugal pumps. *Drain. Irrig. Mach.* **1988**, *6*, 13–17.
6. Kergourlay, G.; Younsi, M.; Bakir, F.; Rey, R. Influence of splitter blades on the flow field of a centrifugal pump: Test-analysis comparison. *Int. J. Rotat. Mach.* **2007**, *13*, 85024. [CrossRef]
7. Gölcü, M.; Pancar, Y.; Sekmen, Y. Energy saving in a deep well pump with splitter blade. *Energy Convers. Manage.* **2006**, *47*, 638–651. [CrossRef]
8. Gölcü, M. Artificial neural network based modeling of performance characteristics of deep well pumps with splitter blade. *Energy Convers. Manag.* **2006**, *47*, 3333–3343. [CrossRef]
9. Gölcü, M.; Usta, N.; Pancar, Y. Effects of Splitter Blades on Deep Well Pump Performance. *J. Energy Res. Technol.* **2007**, *129*, 169–176. [CrossRef]
10. Shigemitsu, T.; Fukutomi, J.; Nasada, R.; Kaji, K. The effect of blade outlet angle on performance and internal flow condition of mini turbo-pump. *J. Therm. Sci.* **2011**, *20*, 32–38. [CrossRef]
11. Shigemitsu, T.; Fukutomi, J.; Wada, T.; Shinohara, H. Performance analysis of mini centrifugal pump with splitter blades. *J. Therm. Sci.* **2013**, *22*, 573–579. [CrossRef]
12. Yuan, S.Q.; Zhang, Y.Z. Tests on centrifugal pump with deviated splitting vanes. *Trans. Chin. Soc. Agric. Mach.* **1995**, *1995*, 79–83.
13. Yuan, S.Q.; Zhang, J.F.; Yuan, J.P.; Fu, D.Y. Orthogonal testal study effect of main geometry factors of splitter blades on pump performance. *J. Drain. Irrig. Mach. Eng.* **2008**, *2008*, 1–5.
14. Yuan, S.Q.; Zhou, J.J.; Yuan, J.P.; Zhang, J.F.; Xu, Y.P. Numerical Simulation on Radial Hydraulic Forces for Screw-type Centrifugal Pump with Splitter Blade. *Trans. Chin. Soc. Agric. Mach.* **2012**, *43*, 37–42.
15. Zhang, J.F. Numerical Forecast and Research on the Design Method for Centrifugal Pumps with Splitter Blades. Ph.D. Thesis, Jiangsu University, Zhenjiang, China, 2007.
16. Zhang, J.F.; Li, G.D.; Mao, J.Y.; Yuan, S.Q.; Qu, Y.F.; Jia, J. Effects of the outlet position of splitter blade on the flow characteristics in low-specific-speed centrifugal pump. *Adv. Mech. Eng.* **2018**, *10*, 1–12. [CrossRef]
17. Gu, Y.D.; Yuan, S.Q.; Pei, J. Effects of the impeller–volute tongue interaction on the internal flow in a low-specific-speed centrifugal pump with splitter blades. *Proc. Inst. Mech. Eng. Part A J. Power Energy.* **2018**, *232*, 170–180. [CrossRef]

18. Cui, B.L.; Chen, F.; Ge, M.Y. Internal flow characteristics and performance test of low specific-speed centrifugal pumps. *J. Drain. Irrig. Mach. Eng.* **2016**, *34*, 375–380.
19. Guo, X.M.; Zhu, L.; Zhu, Z.C. Numerical and experimental investigations on the cavitation characteristics of a high-speed centrifugal pump with a splitter-blade inducer. *J. Mech. Sci. Technol.* **2015**, *29*, 259–267. [CrossRef]
20. Yuan, Y.; Yuan, S.Q. Analyzing the effects of splitter blade on the performance characteristics for a high-speed centrifugal pump. *Adv. Mech. Eng.* **2017**, *9*, 1–11. [CrossRef]
21. Jia, Y.; Wei, X.; Wang, Q.; Cui, J.; Li, F. Experimental Study of the Effect of Splitter Blades on the Performance Characteristics of Francis Turbines. *Energies* **2019**, *12*, 1676. [CrossRef]
22. Wang, F.J. *Principle and Application of CFD Software for Computational Fluid Dynamics Analysis*; Tsinghua University Press: Beijing, China, 2004; pp. 110–130.
23. Menter, F.R. Zonal two equation k-turbulence models for aerodynamic flows. *Am. Inst. Aeronaut. Astronaut. Pap.* **1993**, *7*, 2906.
24. Menter, F.R. Ten years of experience with the SST turbulence model. *Turbul. Heat Mass Transf.* **2003**, *4*, 625–632.
25. Xie, L.H.; Zhao, X.Y. *ANSYS CFX Fluid Analysis and Simulation*; Publishing House of Electronics Industry: Beijing, China, 2013; pp. 12–19.
26. Dai, C.; Kong, F.Y.; Dong, L. Pressure fluctuation and its influencing factors in circulating water pump. *J. Cent. South Univ.* **2013**, *20*, 149–155. [CrossRef]
27. Wang, A.M.; Wen, J. Application for Optimal Designing of Interior Permanent Magnet Synchronous Machines by Using Taguchi Method. *J. North Chin. Electr. Power Univ.* **2016**, *43*, 39–44.
28. Ahmadzadeh, M.; Mortazavi, S.; Saniei, M. Applying the Taguchi Method for Investigating the Phase-Locked Loop Dynamics Affected by Hybrid Storage System Parameters. *Energies* **2018**, *11*, 226. [CrossRef]